Title: Coherent acoustic phonons generated by ultrashort terahertz pulses in nanofilms of metals and topological insulators

Author: A. Levchuk, Bartosz Wilk, G. Vaudel, F. Labbé, B. Arnaud, Katarzyna Balin, Jacek Szade i in.

Citation style: Levchuk A., Wilk Bartosz, Vaudel G., Labbé F., Arnaud B., Balin Katarzyna, Szade Jacek i in. (2020). Coherent acoustic phonons generated by ultrashort terahertz pulses in nanofilms of metals and topological insulators. “Physical Review B” (Vol. 101 (2020), Art. No. 180102), doi 10.1103/PhysRevB.101.180102

Rapid Communications

Coherent acoustic phonons generated by ultrashort terahertz pulses in nanofilms of metals and topological insulators

A. Levchuk,[1] B. Wilk,[2] G. Vaudel,[1] F. Labbé,[1] B. Arnaud,[1] K. Balin,[2] J. Szade,[2] P. Ruello,[1] and V. Juvé[1,*]

[1]*Institut des Molécules et Matériaux du Mans, UMR 6283 CNRS, Le Mans Université, Avenue Olivier Messiaen, 72085 Le Mans, France*

[2]*A. Chełkowski Institute of Physics and Silesian Center for Education and Interdisciplinary Research, University of Silesia, 75 Pułku Piechoty 1A, 41-500 Chorzów, Poland*

(Received 8 January 2020; accepted 28 April 2020; published 18 May 2020)

We report the generation of coherent acoustic phonons in materials with terahertz ultrashort pulses. This is demonstrated in metals and topological insulators by exciting an acoustic eigenmode in nanometric-sized thin films. The efficiency of the coupling is quadratic in the terahertz electric field strength within the range of investigation. Owing to a quantitative comparison between terahertz and near-infrared ultrashort pulse excitations, we show that the process of acoustic phonon generation by terahertz radiation is mainly driven by thermoelastic stress. While for the near-infrared light excitation the lattice temperature increase comes from a rapid energy transfer from the hot carriers to the phonon bath during carrier intraband relaxation, the thermoelastic stress induced by the terahertz electric field is linked to the scattering of the accelerated electrons leading to an ultrafast Joule effect.

DOI: 10.1103/PhysRevB.101.180102

Intense picosecond terahertz radiation has opened new opportunities in solid state physics and materials science to probe and/or to control different degrees of freedom of a solid by driving electrons, magnons, or phonons at ultrafast timescales with an intense electric field associated with a photon energy in the meV range [1–6]. Owing to significant spectral weight in the terahertz (THz) frequency range and to the momentum conservation, THz light can couple directly to infrared active phonon modes [7–10]. While optical phonons driven by THz pulses have been already explored and discussed, only a few reports of THz-driven coherent acoustic phonons exist so far by using momentum and/or energy conversation of THz radiation [11,12] and only one by using picosecond THz pulses but lacking a clear demonstration [13].

In nonpiezoelectric and absorbing materials, the photoinduced generated strain (i.e., coherent acoustic phonons) is usually initiated by thermoelasticity or by the deformation potential stress. The thermoelastic process ($\Delta\sigma_T$) is related to a rapid thermal expansion of the lattice after the photoexcited electron subsystem has transferred its energy to the phonon subsystem, leading to an increase of the lattice temperature ΔT_L (i.e., incoherent phonon population) [14–16]. The deformation potential photoinduced stress ($\Delta\sigma_e$) is driven by the modification of the interatomic potential induced by the photoexcited electrons (i.e., electronic pressure) [14–16]. It is known that for femtosecond near-infrared (NIR) excitation in metals [14–18] such as chromium [19] or aluminum, the incoherent phonon contribution to the elastic strain, and thus to the generation of coherent acoustic phonons, prevails on the electronic contribution for hundreds of gigahertz (GHz) coherent acoustic phonons [$\Delta\sigma_T \gg \Delta\sigma_e$; see Fig. 1(b) [20]]. This process takes place during hot carrier intraband relaxation, leading to a temperature increase (ΔT_L) of the lattice following direct optical transitions [see Fig. 1(a)]. In contrast, a pulsed THz electric field accelerates electrons, which undergo multiple collisions and scattering at the Fermi level (few meV above the Fermi level) contributing to an overall rise of the lattice temperature inducing thermoelastic stress [Joule effect; see Fig. 1(a)]. An intense THz electric field can as well distort the band structure and the electrons' distribution, which contributes to the deformation potential stress. Despite these expectations, conclusive experimental reports on acoustic phonon generation and discussions of such mechanisms are lacking to either confirm or deny these scenarios for the THz excitation regime.

In this Rapid Communication, we evidence the generation of coherent acoustic phonons in materials with terahertz ultrashort pulses. We show that the process of acoustic phonon generation by terahertz radiation is mainly driven by thermoelastic stress induced by the scattering of the accelerated electrons leading to an ultrafast Joule effect. From a fundamental point of view, this possibility should allow to control the solid's macroscopic pressure associated with the acoustic phonon field, which is not a unit cell strain limited as in the case of THz-driven optical phonons. Understanding the generation of acoustic phonons by THz pulses is also important for THz photonics applications since acoustic phonons can be a source of noise or decoherence in the field of optomechanics. Regarding the technological applications, generating coherent GHz-THz acoustic phonons with picosecond THz

*vincent.juve@univ-lemans.fr

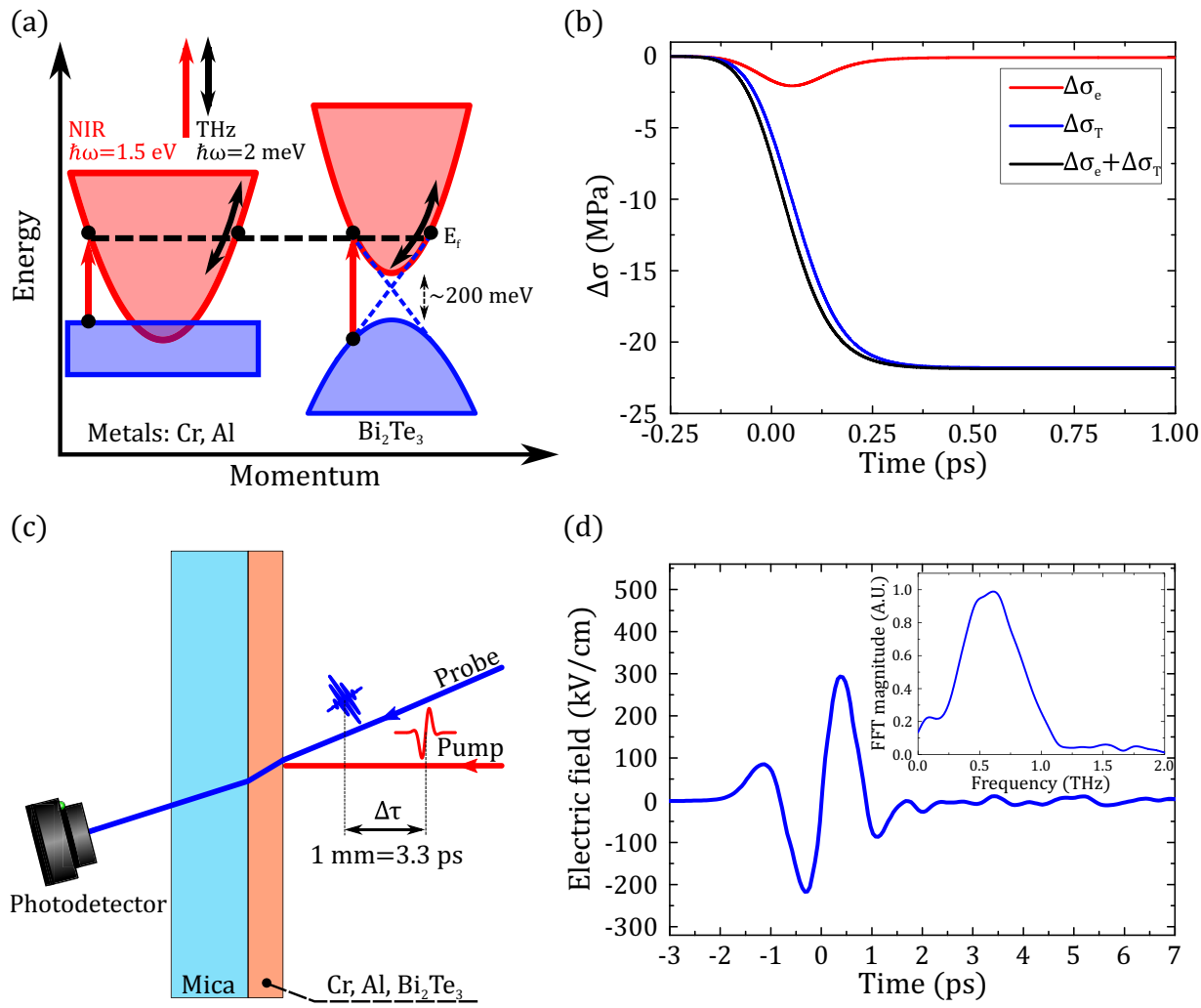

FIG. 1. (a) Simplified electronic band structure of the metal and of the degenerated *n*-doped Bi_2Te_3. Simple vertical arrows show the interband optical transition induced by the NIR pulse and double black arrows represent carrier intraband acceleration by the THz electric field. The blue dashed lines represent the spin-polarized Dirac surface states. (b) Dynamic of the photoinduced stresses originating from the electrons ($\Delta\sigma_e$) or from the phonons ($\Delta\sigma_T$) in the case of the prototypical metal aluminum. The NIR light pulse duration is 165 fs, the absorbed energy is $\sim$10 J/cm^3, and the thickness is 20 nm. (c) Sketch of the femtosecond time-resolved experiment. (d) Temporal trace of the THz driving field along with its spectrum components (inset).

light should open different perspectives for probing elasticity and viscoelasticity of soft matter as it does not suffer optical damage as in the case of visible or NIR light.

In order to investigate the THz-induced coherent acoustic phonon generation, we carried out THz ultrafast experiments on prototypical metals (chromium and aluminum) and the topological insulator bismuth telluride (Bi_2Te_3) to open different perspectives towards correlated materials. Their electronic band structures are sketched in Fig. 1(a). The metals are thin films obtained by pulsed-vapor deposition on a transparent mica substrate with the thicknesses of $H = 14 \pm 0.5$ nm (Cr) and $H = 20 \pm 0.5$ nm (Al) and were measured by x-ray reflectivity. Thin Bi_2Te_3 films with various thicknesses ranging from 4 to 25 nm were also studied, which were grown by molecular beam epitaxy on a transparent mica substrate. Details about the preparation can be found in previous works [21–23]. We remind that Bi_2Te_3 is a narrow band gap semiconductor ($E_g \sim 0.2$ eV) with spin-polarized Dirac surface states. However, the system studied here is Te rich and consequently is an *n*-doped Bi_2Te_3 with a Fermi level in the conduction band [21]. The presence of free carriers at the Fermi level has been verified with ultraviolet photoemission spectroscopy (see Supplemental Material [24]). The experiments make use of an ultrafast THz pump and visible probe scheme in the transmission geometry as depicted in Fig. 1(c). The THz pulses are generated by optical rectification in a $LiNbO_3$ crystal [25,26] and its temporal evolution was characterized by electro-optic sampling in a 200-μm-thick GaP crystal [shown along with its frequency components in Fig. 1(d)]. The maximum focused THz electric field used in the experiment was estimated to be around 275 kV/cm [26] ($1/e^2$ radius of $\sim$615 μm measured by a knife-edge method), which corresponds to a pulse energy of roughly 1.2 μJ measured by a calibrated pyroelectric detector. The THz ultrafast experiments were compared to NIR (1.55 eV) pump/probe measurements. In both experiments (THz and

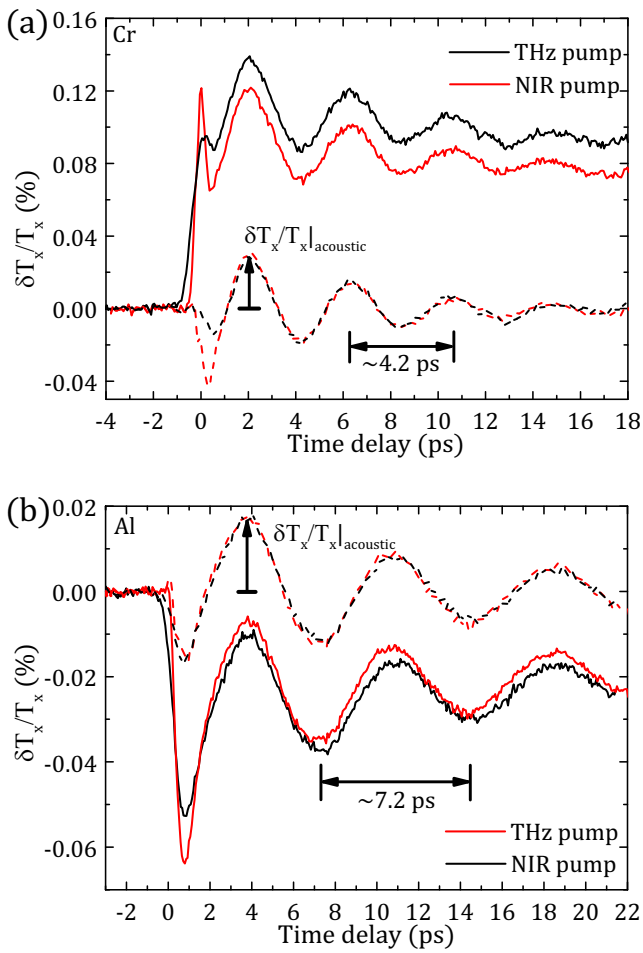

FIG. 2. (a) Transient optical transmission obtained with a THz or NIR pump excitation for a thin Cr film. Dashed lines correspond to the extracted oscillatory parts of the signals (see text). The pulse energy of the NIR is ~0.07 μJ and the THz peak electric field is ~275 kV/cm. (b) Same as (a) but for a thin 20-nm Al film. The pulse energy of the NIR pulse is ~0.04 μJ and the THz peak electric field is ~250 kV/cm.

NIR excitations), the probe wavelength has been kept to the same energy, 3.1 eV (400 nm), in order to avoid spurious effects due to the detection process. The pump-induced probe transmission change ($\delta T_x/T_x$) reflects the structural change of the samples as a function of the time delay.

The first ultrafast THz pump and visible probe experiment is performed on a chromium thin film and is shown in black in Fig. 2(a). The transient consists of a sharp rise of the probe's optical transmission subsequent to the THz excitation followed by a slower decay related to the lattice excess energy and thus to the lattice temperature elevation (ΔT_L, incoherent phonons). On top of this thermal background a clear oscillatory feature is present. An iterative fitting procedure allows us to isolate only the oscillatory component, which has a temporal period of about 4.2 ps ($f_{Cr} \approx 238$ GHz), as well as its amplitude ($\delta T_x/T_x|_{acoustic}$) and phase. The period of the oscillatory signal is attributed to the acoustic eigenmode (breathing mode) of the Cr layer whose frequency is $f_{Cr} = V_{Cr}/2H$, where V_{Cr} is the longitudinal sound velocity in chromium and H is the thickness [27]. From our measurements, we deduce $V_{Cr} \approx 6600$ m/s, which is in good agreement with the literature [19]. The signal obtained with NIR excitation [in red in Fig. 2(a)] has a similar transient's general shape (coherent and incoherent phonons) except for the fast rise and fall of the probe's optical transmission at short timescales ($\tau < 1$ ps) associated with the electron-phonon scattering. The extracted period and phase of the coherent acoustic mode are equivalent to the ones measured upon THz excitation. Similar results have been obtained with a thin aluminum film [Fig. 2(b)], which, contrary to chromium, has no magnetic properties, therefore ruling out a possible contribution of the magnetostriction mechanism. The observed acoustic phonon mode has a frequency of 139 GHz in accordance with the measured film thickness and the longitudinal sound velocity ($V_{Al} \approx 6320$ m/s). For both samples and the two different excitation wavelengths, Brillouin oscillations at a frequency of 35 GHz were observed in the mica substrate [16].

Figure 3(a) displays the amplitude of the coherent acoustic phonon mode ($\delta T_x/T_x|_{acoustic}$) as a function of the THz peak electric field and is found to vary quadratically [linearly as a function of the pulse energy; see the inset of Fig. 3(a)]. The measured linearity of $\delta T_x/T_x|_{acoustic}$ as a function of the THz pulse energy excludes highly nonlinear processes such as impact ionization or Zener tunneling [28,29]. The same linear dependence is found for the NIR excitation. From a microscopic point of view, the long pulse duration and the low frequency of the THz pulse leads to a time-dependent absorbed density of energy by the electrons, which can be expressed as

$$W_{Abs.}^{THz}(t) = \int_{-\infty}^{t} \vec{E}_{loc}(t') \cdot \vec{j}(t')dt', \quad (1)$$

with $j(t') = \int_{-\infty}^{t'} \sigma(t'-t'')E_{loc}(t'')dt''$, the current density. $E_{loc}(t)$ and $\sigma(t)$ are the local THz electric field acting on the electrons and the time-dependent electrical conductivity, respectively. We measured the dielectric function in the THz frequency range of our samples by time-domain THz spectroscopy [30] and extracted a plasma frequency $w_p \approx 350$ THz and an electronic scattering rate $\Gamma \approx 14$ THz for the Cr thin film (see Supplemental Material [24]). These parameters lead to a nearly-frequency-independent conductivity $\sigma \approx 4.5 \times 10^5\ \Omega\,m^{-1}$ for our THz frequency range and therefore we neglect the retardation effects. As the characteristic scattering frequency in metals is typically well above the frequency of our driving THz field, we limit our model to the stationary drift electron transport regime neglecting any ballistic transport effect. Moreover, as our samples are much thinner than the driving field's wavelength, the local electric field can be approximated by the electric field inside the sample $E_{in}(t)$. The finite domain time difference method was then implemented [31,32] to simulate the electric field in the vacuum, sample, and substrate. It allows us to calculate the electric field inside the sample by $E_{in}(t) = sE(t)$, with $E(t)$ the vacuum THz electric field and $s \approx 0.45$ the electric field attenuation coefficient. Using Eq. (1) and the experimental parameters, the absorbed energy was found to be $W_{Abs.}^{THz} \approx 52$ J cm^{-3} for the highest THz electric field possible in our experiments [Fig. 3(b)]. This value corresponds to a lattice

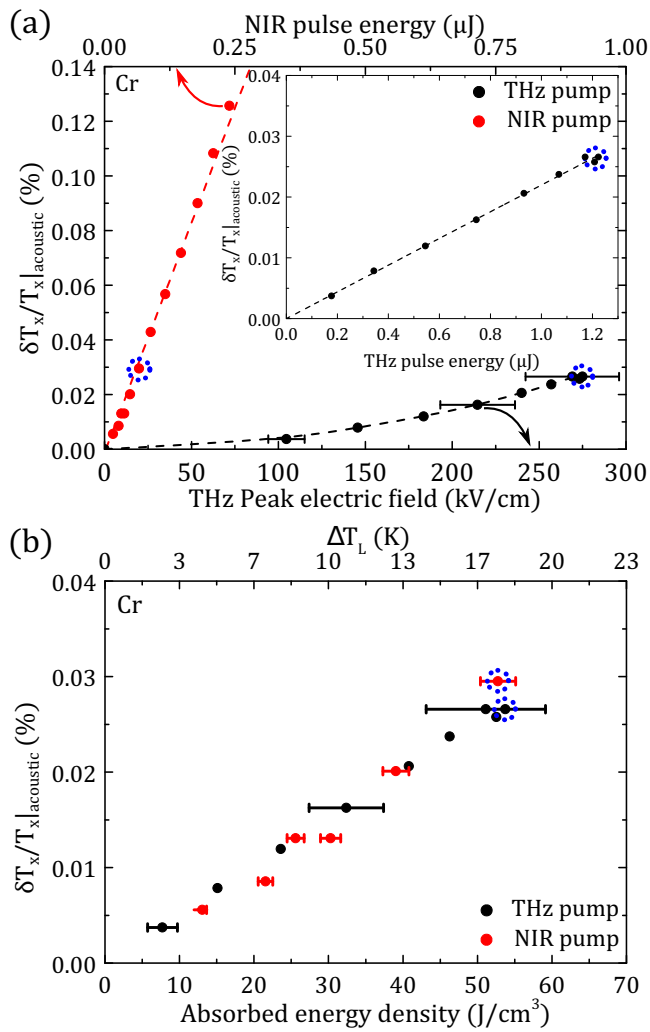

FIG. 3. (a) THz peak electric field and NIR pulse energy dependence of the acoustic phonon signal for the Cr thin film. The blue circles indicate the transients shown in Fig. 2(a). Inset: Coherent acoustic phonon amplitude vs THz pulse energy. (b) Acoustic phonon amplitude as a function of the absorbed density energy for the Cr sample. The THz absorbed energy was calculated by using Eq. (1). The blue circles indicate the transients shown in Fig. 2(a).

temperature elevation of $\Delta T_L^{\mathrm{THz}} \sim 17$ K [33]. In contrast, direct optical transitions induced by NIR excitation lead to an absorbed energy expressed by $W_{\mathrm{Abs.}}^{\mathrm{NIR}} = ANh\nu_{\mathrm{NIR}}/V$, with A the absorption coefficient, N the number of photons of energy $h\nu_{\mathrm{NIR}}$, and V the excited volume [34]. Remarkably, we obtain an equivalent coherent acoustic phonon amplitude with NIR excitation compared to THz excitation with a similar absorbed energy of $W_{\mathrm{Abs.}}^{\mathrm{NIR}} \approx 53$ J cm^{-3}. Moreover, this evidence is verified over the entire absorbed energy range [Fig. 3(b)].

Considering that the generation of hundreds of GHz acoustic phonons in metals with NIR light pulse is known to originate from thermoelastic stress [16] [see Fig. 1(b)], the comparable contribution of the coherent acoustic phonons and the incoherent phonons to the experimental signal for THz excitation with similar absorbed energy strongly suggests that thermoelastic stress is the main physical mechanism for the acoustic phonon generation ($\Delta\sigma_T^{\mathrm{THz}} > \Delta\sigma_e^{\mathrm{THz}}$). This confirms our modeling of dissipation of the electrons' kinetic energy driven by the THz electric field via ultrafast scattering leading to an increase of the incoherent phonon population. Even if the THz and NIR excitations involve different relaxation mechanisms, the characteristic time of incoherent phonon population increase (i.e., lattice heating) is similar in both cases (THz electric field duration and electron-phonon coupling time) and is much smaller that the measured coherent acoustic phonon period. As such, we cannot discriminate between the two electronic relaxation channels contrary to the rapid rise-and-fall signal in the early stage of excitation for NIR and THz observed in Fig. 2(a).

We extended our experiments to n-doped Bi_2Te_3, as shown in Figs. 4(a)–4(d), with a Fermi level in the conduction band well above the Dirac cones (see Supplemental Material [24]). Considering the light penetration depth in Bi_2Te_3, the optical techniques used in this study are not specifically sensitive to Dirac surface states contrary to angle-resolved photoemission spectroscopy [36,37]. Therefore all the interpretations will be reasonably done without taking into account these surface states. In Fig. 4(a), the signal of the Bi_2Te_3 layer is shown with the THz and NIR pump pulse energy fixed at 1.2 μJ and 51 nJ, respectively. In both types of excitations, the transient optical transmission $\delta T_x/T_x$ shows a sharp variation after the initial excitation and a fast recovery followed by a slower decaying signal linked to the thermal background. The fast recovery signal is related to the relaxation of hot carriers and is characterized by a decay time constant of about 1.8 ps in accordance with previous ultrafast optical spectroscopy experiments [36,38,39]. On top of these signals, two frequencies are clearly evidenced: a fast oscillatory component at around 1.8 THz, which is attributed to the Raman active $A_{1g}^{(1)}$ optical phonon (already studied in Bi_2Se_3 [8] and will not be discussed in this Rapid Communication) and a slower of acoustic nature at 85 GHz. The amplitude of the acoustic coherent phonons scales linearly with the THz pulse energy [Fig. 4(b)]. We have tuned the thickness of the Bi_2Te_3 films and the corresponding signals are shown in Figs. 4(c) and 4(d). We clearly observe the thickness dependence of the GHz mode, which perfectly confirms that it is a longitudinal acoustic eigenmode as we observed for the thin metallic films. The highest coherent acoustic phonon frequency was found to be ~250 GHz for our thinnest sample. The estimated sound velocity of roughly 2700 m/s is in agreement with previous reports [22,23]. Similar results are obtained with NIR excitation (not shown). The linear pump pulse energy dependence of the acoustic phonon amplitude [Fig. 4(b)] shows that highly nonlinear field effects such as impact ionization or the Zener tunneling effect [28,29] may be ruled out as in the case of metals. The same long-term residual signal for the THz and NIR excitation indicates that the process of coherent acoustic phonon generation might be the same for both kinds of excitation. Moreover, the evolution of the phase of the coherent acoustic phonons as a function of the samples' thicknesses [inset of Fig. 4(d)] might indicate a change in the excitation process [40] or a change in the electronic band structure [23,39]. At this stage, we cannot conclude about the physical origin of the light-induced coherent acoustic phonon generation in n-doped topological insulators.

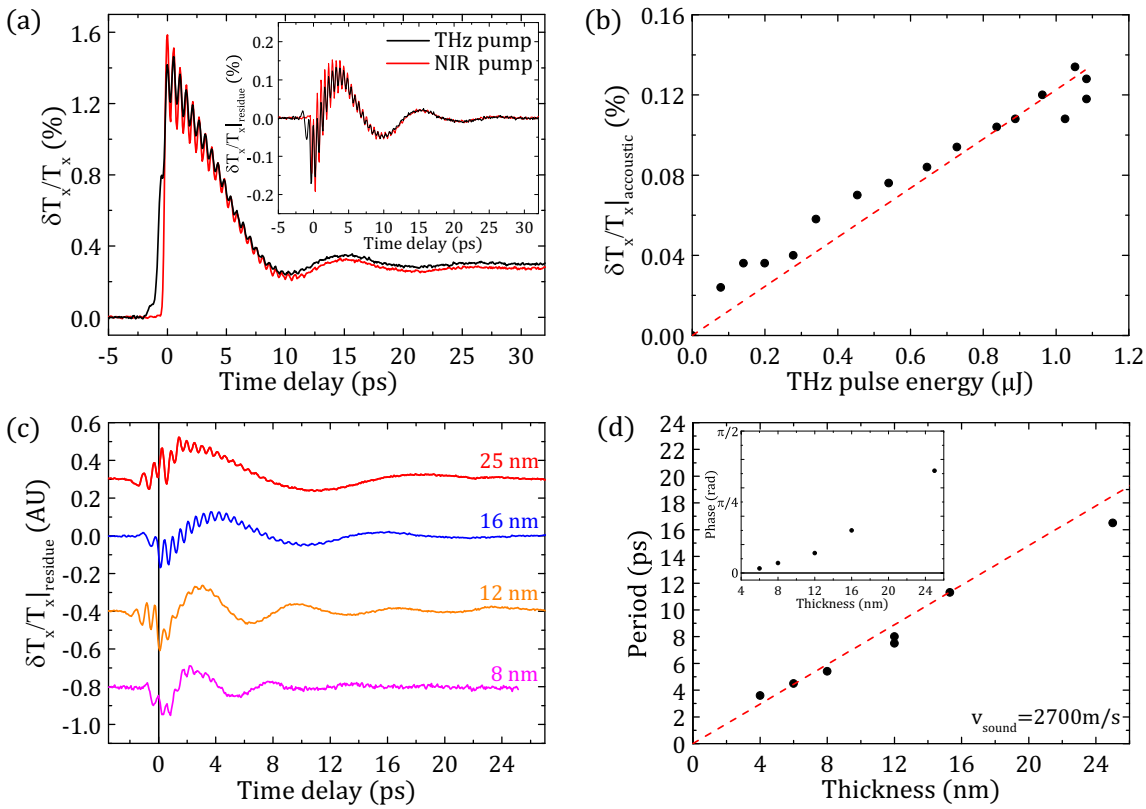

FIG. 4. (a) Transient optical transmission obtained with a THz or NIR pump excitation for a 15-nm Bi_2Te_3 thin film with 51 nJ and 1.2 μJ for NIR and THz excitation, respectively. Inset: Oscillatory part of the signal. (b) THz pulse energy dependence of the acoustic phonon amplitude for the 15-nm thin film. (c) Thickness dependence of the coherent acoustic phonon signal generated by THz excitation. (d) Coherent acoustic phonon oscillation period vs the film thickness. Inset: Phase of the coherent acoustic phonon respect to a cosine function as a function of the samples' thicknesses.

Contrary to metals, the existence of long-lived carriers due to the band gap (even small) and the large deformation potential constant [22,23] could benefit a nonthermal process such as photoinduced deformation potential stress ($\Delta\sigma_e$). In addition, preliminary first-principles calculations also reveal a possible contribution to the coherent acoustic phonon generation from the electrostriction mechanism, which depends linearly on the pump energy [14–16]. At this stage, more experimental work with various carrier dopings and controlled Fermi levels would help to disentangle the different generation mechanisms involved. For example, low-temperature ultrafast THz investigations can be carried out as they will reduce the amount of thermally activated carriers in the conduction band due to the small band gap of our samples ($E_g \sim 0.2$ eV).

In conclusion, we have evidenced the generation of coherent acoustic phonons in metallic and topological insulator thin films with an ultrashort THz light pulse. The efficiency of the coupling is quadratic in the THz electric field strength (linear with the pulse energy) within the range of investigation. A direct comparison with a NIR femtosecond excitation permits us to demonstrate that the thermoelastic process is the driving mechanism for metals but with a distinguished microscopic mechanism. While for NIR excitation the ultrafast lattice heating is achieved by intraband hot electron relaxation, THz-induced near Fermi multiple electron-phonon scattering processes are responsible for the lattice temperature increase (ultrafast Joule effect). Although the relaxation channels are different, we demonstrate that they do not have an impact on the coherent acoustic phonon generation for the relatively low-frequency range of interest. Studying higher acoustic frequencies should permit us to reveal the very different nature of heating based either on intraband relaxation or by multiple electron scattering at the Fermi level, which could be done by investigating nanoparticles with various sizes [18]. In topological insulator nanofilms, experimental evidence indicates that the generation process might be the same for both kinds of excitation due to the presence of free carriers. The generation of coherent acoustic phonons by an ultrashort THz pulse could open other fundamental opportunities for controlling the solid's macroscopic pressure as well as different technological interests for probing elasticity or viscoelasticity in soft matter.

We acknowledge financial support by the French National Research Agency: SANTA-ANR-18-CE24-0018-03 and International laboratory LIA IM-LED. B.W., J.S., and K.B. acknowledge the support from National Science Center under Project No. 2016/21/B/ST5/0253. A.L. would like to thank the Ecole Doctorale 3MPL (Matière, Molécules et Matériaux, Pays de la Loire France) for support from a Ph.D. grant.

Calculations were performed using HPC resources from GENCI-CINES (Project No. 095096). We thank Mathieu Edely for the preparation of thin metallic films. P.R. and V.J. thank A. Maznev for fruitful discussions.

[1] T. Kampfrath, K. Tanaka, and K. A. Nelson, Nat. Photonics **7**, 680 (2013).
[2] W. Kuehn, P. Gaal, K. Reimann, M. Woerner, T. Elsaesser, and R. Hey, Phys. Rev. Lett. **104**, 146602 (2010).
[3] T. Kampfrath, A. Sell, G. Klatt, A. Pashkin, S. Mahrlein, T. Dekorsy, M. Wolf, M. Fiebig, A. Leitenstorfer, and R. Huber, Nat. Photonics **5**, 31 (2011).
[4] O. Schubert, M. Hohenleutner, F. Langer, B. Urbanek, C. Lange, U. Huttner, D. Gold, T. Meier, M. Kira, S. W. Koch, and R. Huber, Nat. Photonics **8**, 119 (2013).
[5] T. Tamaya, A. Ishikawa, T. Ogawa, and K. Tanaka, Phys. Rev. Lett. **116**, 016601 (2016).
[6] S. Baierl, M. Hohenleutner, T. Kampfrath, A. K. Zvezdin, A. V. Kimel, R. Huber, and R. V. Mikhaylovskiy, Nat. Photonics **10**, 715 (2016).
[7] P. Bowlan, J. Bowlan, S. A. Trugman, R. Valdes Aguilar, J. Qi, X. Liu, J. Furdyna, M. Dobrowolska, A. J. Taylor, D. A. Yarotski, and R. P. Prasankumar, Optica **4**, 383 (2017).
[8] A. A. Melnikov, K. N. Boldyrev, Y. G. Selivanov, V. P. Martovitskii, S. V. Chekalin, and E. A. Ryabov, Phys. Rev. B **97**, 214304 (2018).
[9] I. Katayama, H. Aoki, J. Takeda, H. Shimosato, M. Ashida, R. Kinjo, I. Kawayama, M. Tonouchi, M. Nagai, and K. Tanaka, Phys. Rev. Lett. **108**, 097401 (2012).
[10] M. Kozina, M. Fechner, P. Marsik, T. van Driel, J. M. Glownia, C. Bernhard, M. Radovic, D. Zhu, S. Bonetti, U. Staub, and M. C. Hoffmann, Nat. Phys. **15**, 387 (2019).
[11] W. Grill and O. Weis, Phys. Rev. Lett. **35**, 588 (1975).
[12] T. E. Wilson, Phys. Rev. B **98**, 220304(R) (2018)
[13] J.-M. Manceau, P. A. Loukakos, and S. Tzortzakis, Appl. Phys. Lett. **97**, 251904 (2010).
[14] C. Thomsen, H. T. Grahn, H. J. Maris, and J. Tauc, Phys. Rev. B **34**, 4129 (1986).
[15] V. E. Gusev and A. Karabutov, *Laser Optoacoustics* (AIP, New York, 1993).
[16] P. Ruello and V. Gusev, Ultrasonics **56**, 21 (2015).
[17] J. H. Hodak, A. Henglein, and G. V. Hartland, J. Chem. Phys. **111**, 8613 (1999).
[18] V. Juvé, A. Crut, P Maioli, M. Pellarin, M. Broyer, N. Del Fatti, and F. Vallée, Nano Lett. **10**, 1853 (2010).
[19] T. Saito, O. Matsuda, and O. B. Wright, Phys. Rev. B **67**, 205421 (2003).
[20] *Ab initio* calculations were performed within the framework of the local density approximation using the QUANTUM ESPRESSO method in order to derive the electronic and phonon stresses and their variations upon the change in the electronic and lattice temperatures. The two-temperature model was then employed to describe nonequilibrium processes arising from laser excitation and estimate the electron and lattice temperatures. The main assumption behind this model is that an electron temperature T_e and a lattice temperature T_l can be defined at any time following the laser pulse arrival. See Supplemental Material [24] for more details.
[21] R. Rapacz, K. Balin, A. Nowak, and J. Szade, J. Cryst. Growth **401**, 567 (2014).
[22] M. Weis, K. Balin, R. Rapacz, A. Nowak, M. Lejman, J. Szade, and P. Ruello, Phys Rev. B **92**, 014301 (2015).
[23] M. Weis, B. Wilk, G. Vaudel, K. Balin, R. Rapacz, A. Bulou, B. Arnaud, J. Szade, and P. Ruello, Sci. Rep. **7**, 13782 (2017).
[24] See Supplemental Material at http://link.aps.org/supplemental/10.1103/PhysRevB.101.180102 for details about the *Ab initio* calculations of the thermal and electronic stresses in aluminum, the calculated light induced phonon spectra, the experimental dielectric function of the chromium sample in the THz range and the ultraviolet photoemission spectroscopy spectrum of the Bi_2Te_3 sample (see also Refs. [41–49]).
[25] H. Hirori, A. Doi, F. Blanchard, and K. Tanaka, Appl. Phys. Lett. **98**, 091106 (2011).
[26] V. Juvé, G. Vaudel, Z. Ollmann, J. Hebling, V. Temnov, V. E. Gusev, and T. Pezeril, Opt. Lett. **43**, 5905 (2018).
[27] As the acoustic impedance of all the material involved here is larger than the acoustic impedance of the substrate ($\rho_{\text{mica}} = 2880$ kg/m^3 and $V_{\text{mica}} \approx 4300$ m/s), the thin-film breathing mode frequency is given by $f = V/2H$.
[28] W. Kuehn, P. Gaal, K. Reimann, M. Woerner, T. Elsaesser, and R. Hey, Phys. Rev. B **82**, 075204 (2010).
[29] H. Hirori, K. Shinokita, M. Shirai, S. Tani, Y. Kadoya, and K. Tanaka, Nat. Commun. **2**, 594 (2011).
[30] N. Laman and D. Grischkowsky, Appl. Phys. Lett. **93**, 051105 (2008).
[31] A. Taflove and S. C. Hagness, *Computational Electrodynamics: The Finite-Difference Time-Domain Method* (Artech House, Boston, 1995).
[32] M. Okoniewski and E. Okoniewska, Electron. Lett. **42**, 503 (2006).
[33] We remind that $\Delta T_L = W_{\text{Abs.}}/C_p$, with C_p the heat capacity. For chromium, $C_p \approx 3 \times 10^6$ J m^{-3} [19].
[34] The NIR absorption coefficient was modeled by the matrix transfer method using tabulated optical constants [35] and agrees with our measurements.
[35] A. D. Rakic, A. B. Djurisic, J. M. Elazar, and M. L. Majewski, Appl. Opt. **37**, 5271 (1998).
[36] Y. H. Wang, D. Hsieh, E. J. Sie, H. Steinberg, D. R. Gardner, Y. S. Lee, P. Jarillo-Herrero, and N. Gedik, Phys. Rev. Lett. **109**, 127401 (2012).
[37] M. Hajlaoui, E. Papalazarou, J. Mauchain, G. Lantz, N. Moisan, D. Boschetto, Z. Jiang, I. Miotkowski, Y. P. Chen, A. Taleb-Ibrahimi, L. Perfetti, and M. Marsi, Nano Lett. **12**, 3532 (2012).
[38] D. Hsieh, F. Mahmood, J. W. McIver, D. R. Gardner, Y. S. Lee, and N. Gedik, Phys. Rev. Lett. **107**, 077401 (2011).
[39] Y. D. Glinka, S. Babakiray, T. A. Johnson, A. D. Bristow, M. B. Holcomb, and D. Lederman, Appl. Phys. Lett. **103**, 151903 (2013).
[40] C. Voisin, N. Del Fatti, D. Christofilos, and F. Vallée, Appl. Surf. Sci. **164**, 131 (2000).
[41] J. P. Perdew and A. Zunger, Phys. Rev. B **23**, 5048 (1981).

[42] P. Giannozzi, S. Baroni, N. Bonini, M. Calandra, R. Car, C. Cavazzoni, D. Ceresoli, G. L Chiarotti, M. Cococcioni, I. Dabo *et al.*, J. Phys.: Condens. Matter **21**, 395502 (2009).
[43] M. Fuchs and M. Scheffler, Comput. Phys. Commun. **119**, 67 (1999).
[44] S. Baroni, S. de Gironcoli, A. Dal Corso, and P. Giannozzi, Rev. Mod. Phys. **73**, 515 (2001).
[45] A. Debernardi, M. Alouani, and H. Dreyssé, Phys. Rev. B **63**, 064305 (2001).
[46] B. Arnaud, S. Lebègue, and G. Raffy, Phys. Rev. B **93**, 094106 (2016).
[47] P. B. Allen, Phys. Rev. Lett. **59**, 1460 (1987).
[48] B. Arnaud and Y. Giret, Phys. Rev. Lett. **110**, 016405 (2013).
[49] R. Nitsche and T. Fritz, Appl. Opt. **43**, 3263 (2004).